Removal of Azo Dyes – Tartrazine, Carmoisine, and Allura Red – from Wastewater using Spirulina Biomass–Immobilized Alginate Beads: Equilibrium, Kinetics, Thermodynamics, Desorption…

Article *in* Desalination and Water Treatment · January 2021

DOI: 10.5004/dwt.2021.27010

CITATION
1

READS
195

2 authors:

Oya Irmak Şahin-Cebeci
Yalova Üniversitesi
22 PUBLICATIONS **53** CITATIONS
SEE PROFILE

Didem Saloglu
Istanbul Technical University
32 PUBLICATIONS **110** CITATIONS
SEE PROFILE

Desalination and Water Treatment
www.deswater.com
doi: 10.5004/dwt.2021.27010

220 (2021) 431–445
April

Removal of azo dyes – tartrazine, carmoisine, and Allura Red – from wastewater using *Spirulina* biomass-immobilized alginate beads: equilibrium, kinetics, thermodynamics, desorption, and reusability

Didem Saloglu[a,*], Oya Irmak Sahin[b]

[a]*Disaster and Emergency Management Department, Disaster Management Institute, Istanbul Technical University, Maslak, Istanbul, Turkey, Tel. +90 2122856656; Fax: +90 212 2856656; email: saloglu@itu.edu.tr*
[b]*Department of Chemical Engineering, Engineering Faculty, Yalova University, Yalova, Turkey, Tel. +90 226 8156190; Fax: +90 2268156190; email: oyairmak@yalova.edu.tr*

Received 5 October 2020; Accepted 31 December 2020

ABSTRACT

In the present study, *Spirulina* microalgae-immobilized alginate beads (Alg-SP) were used as novel adsorbents for the adsorption of tartrazine, carmoisine, and Allura Red azo-dyes from wastewater. Synthesized Alg-SP beads were characterized by Fourier-transform infrared spectroscopy, X-ray diffraction, scanning electron microscopy, thermogravimetric analysis, and differential scanning calorimetry analyses. Maximum azo-dye removal percentages were achieved using 100 mg of Alg-SP beads with a ratio of 3.0% (w/v) within 2 h, and tartrazine, carmoisine, and Allura Red removal performances were determined to be 98%, 93%, and 82%, respectively. The adsorption data for azo-dyes onto Alg-SP beads were evaluated by several isotherm equations such as Langmuir, Freundlich, Dubinin–Radushkevich, Temkin, Halsey, and Harkins–Jura isotherm models, but were best described by the Langmuir and Harkins–Jura models as they gave the highest correlation. Pseudo-first-order, pseudo-second-order, Elovich, Weber–Morris, and Bangham models were investigated and dye adsorption onto Alg-SP beads was represented by pseudo-second-order and Elovich kinetic models. After the adsorption process, the beads can easily be regenerated by NaOH and effectively reused over three cycles. Consequently, *Spirulina* microalgae-immobilized alginate beads have considerable potential for the adsorption of dyes from wastewater.

Keywords: Spirulina; Alginate; Adsorption; Azo dyes

1. Introduction

Dyes are widely used organic chemicals to give products "color", especially in food, pharmaceutical, textile, paper, leather, and cosmetic industries. Dyes have a complex aromatic molecular structure, which is based on substituted aromatic and heterocyclic groups, and are generally resistant to light, temperature, biodegradation, ozonation, and oxidation [1,2]. This characteristic feature makes dyes non-degradable and therefore causes bioaccumulation in living organisms, leading to severe diseases and disorders. In addition, dyes may have acute or chronic effects on organisms in water [3]. Moreover, toxic dyes can enter the food chain through water bodies, eventually affecting the health of humans and animals. Some studies demonstrated the allergenic, clastogenic, mutagenic, and carcinogenic effects of different dyes, such as tartrazine, amaranth, Allura Red, carmoisine, and brilliant blue [4].

Tartrazine is a synthetic lemon yellow azo dye used as a food coloring. This dye provokes asthma attacks in children and when combined with benzoates, it can produce hyperactivity syndrome and thyroid tumors. It also causes agitation, infertility, confusion, rhinitis, and migraine.

* Corresponding author.

Overdose of tartrazine in people displays effects on peripheral nerves, paraesthesia and dental changes. Food and Agriculture Organization/World Health Organization (FAO/WHO) established an acceptable daily intake for tartrazine of 7.5 mg kg^{-1} b.w. d^{-1}. Carmoisine is an azo dye with red color [4]. It is reported that an excess dose of carmoisine damages the liver and decreases the function of some main metabolic enzymes. Carmoisine is reported to produce carcinogenicity and biochemical toxicity in mice by increasing the concentration of some serum marker enzymes and downregulating the expression of some important defensive genes. FAO/WHO established an acceptable daily intake for carmoisine of 4.0 mg kg^{-1} b.w. d^{-1} [5]. Allura Red is an azo dye used in the food industry. Use of Allura Red over 7.0 mg kg^{-1} causes toxicity and carcinogenicity, which can lead to several diseases such as bladder cancer. Allura Red overdose reduces intestinal anaerobic bacteria. The acceptable daily intake value for Allura Red in food is 7.0 mg kg^{-1} b.w. d^{-1} [6].

Removing dyes from contaminated water has become an urgent requirement. The adsorption process is one of the efficient methods to remove dyes from effluent. Adsorption is the most commonly used technology for the removal of dyes, due to its simple design and easy operation [7]. Using an efficient adsorbent is an important parameter in the adsorption process for dye removal with high adsorption capacity. Nowadays, a number of low-cost, commercially available adsorbents are used for dye removal. Various adsorbents, which are low-cost materials such as natural clays, activated carbon, chitosan, alginate, microalgae biomass, etc. have been reported for dye adsorption [8]. Also, organic/inorganic compounds containing polymeric composites with high adsorption capacity and removal ratio are the precursors in the search for new adsorbents lately.

Alginate is a linear polysaccharide, which was used for the removal of various pollutants such as pharmaceuticals, food, and textile dyes in recent decades [9]. In addition, the blue-green microalgae *Spirulina platensis* is the most industrially cultivated microalgae since its biomass is widely used as food, feed, and a source of fine chemicals. Its biomass contains significant amounts of protein, precious fatty acids, and complex carbohydrates [10]. These nutritional chemical groups make *Spirulina* biomass a good source for a variety of functional groups such as carboxyl, hydroxyl, sulfate, and phosphate that can be used as binders for dye adsorption [11]. *Spirulina* biomass stands out due to its high adsorption capacity and its availability in natural surroundings, in addition to offering a variety of functional groups, being low-cost and ecologically beneficial. The powdered form of *Spirulina* presents advantages in operation such as mechanical characteristics and removal from the liquid medium after adsorption [12].

The objective of the present paper is to evaluate whether introducing *Spirulina* biomass into the polymeric structure of alginate can significantly enhance the surface area of the alginate and promote the adsorption capacity of the polymer for the removal of dyes from wastewater. The chemical and morphological properties of the beads were characterized, and the effect of adsorption parameters such as amount of *Spirulina* biomass, amount of adsorbent, pH, temperature, and time was investigated. The Langmuir, Freundlich, Temkin, Dubinin–Radushkevich (D–R), Halsey, and Harkins–Jura adsorption isotherms and pseudo-first-order, pseudo-second-order, Elovich, Weber–Morris, and Bangham kinetics models were studied. The thermodynamic parameters were evaluated, and also enthalpy, entropy, Gibbs free energy, adsorption mechanism, desorption, and reusability experiments were also carried out. This work represents the first example in the literature to present the synthesis, characterization and dye adsorption behavior of *Spirulina* biomass immobilized on alginate beads.

2. Material and method

2.1. Microorganism and cultivation

The cyanobacterium *Arthrospira* (*Spirulina*) *platensis* (SP) was cultivated on Zarrouk's medium in 2 L photobioreactors with an initial biomass concentration of 0.15 g L^{-1} [10]. Cultures were maintained under a 12 h light/12 h dark photoperiod at 25°C ± 1°C. At the end of the 25 d cultivation, cultures were filtered, washed with distilled water, centrifuged at 10,000 rpm, and freeze-dried to obtain biomass.

2.2. Preparation of Spirulina-immobilized alginate beads

Amounts of 1.0% (w/v) sodium alginate and 1.0, 2.0 and 3.0% (w/v) dried *Spirulina* were dissolved in 0.1 M NaCl solution for 24 h. The alginate-*Spirulina* (Alg-SP) solutions were added dropwise to 0.1 M $CaCl_2$ solution using a plastic syringe and left on a magnetic stirrer for 24 h at 25°C. The obtained Alg-SP wet beads were separated from the solution and washed using distilled water. Finally, Alg-SP beads were dried in an oven at 60°C for 24 h and coded as Alg-SP-1.0, Alg-SP-2.0, and Alg-SP-3.0 [9].

2.3. Characterization

The molecular structures of raw SP, raw alginate and Alg-SP beads were characterized by IR Affinity Spectrometer (Perkin Elmer, Turkey). X-ray diffraction measurements of raw SP, raw alginate and Alg-SP beads were conducted on a RIGAKU D-Max 2200 (Japan) ultimate diffractometer. Scanning electron microscopy (Philips XL-30, United States) was used to observe the surface morphologies of raw SP, raw alginate, and Alg-SP beads. Thermal characterization of the beads was carried out by thermogravimetric analysis (TG, Perkin Elmer, Turkey), and differential scanning calorimetry (Diamond DSC, Turkey). The points of zero charges (PZC) of the beads were established using the salt addition method [9,13].

2.4. Preliminary adsorption experiments

In batch adsorption experiments, 25 mL of 50 mg L^{-1} dye solutions with pH from 3.0 to 11.0 were added to 50–200 mg of Alg-SP-(1.0:3.0) in a 50 mL Erlenmeyer at 25°C ± 0.5°C on a mechanical shaker at 140 rpm for 1 h [9,13,14]. Then Alg-SP beads were separated from the solution and the residual concentrations of the dyes in the supernatant were monitored with a double-beam spectrophotometer at 426 nm for tartrazine, 508 nm for

carmoisine, and 501 nm for Allura Red. Adsorption experiments were repeated three times, and the standard deviations were within ca. ±3%, so all results are reproducible.

Adsorption isotherms for dyes onto Alg-SP-3.0 beads were described with different models, namely the Langmuir, Freundlich, D–R, Temkin, Halsey, and Harkins Jura models. Similarly, adsorption kinetics experiments were carried out using 100 mg of Alg-SP-3.0 beads at different time intervals and the adsorption kinetics were investigated by pseudo-first-order, pseudo-second-order, Elovich, Weber–Morris, and Bangham models. The experiments were carried out at 25°C, 45°C and 60°C ± 0.5°C to examine the adsorption thermodynamics [15].

Desorption studies were conducted by suspending the Alg-SP-3.0 beads loaded with dyes in distilled water at different pH values (3.0–12.0) with 1.0 M HCl, and NaOH solutions as eluent solutions. The dye-loaded beads and 25 mL of eluents were shaken for 1 h and the residual dye concentration was measured spectrophotometrically. The desorption efficiencies of dyes were calculated as the ratio of the desorbed amount to the adsorbed amount [16]. Five cycles of consecutive adsorption–desorption studies were performed for all dyes in order to check the reusability of the regenerated beads.

3. Results and discussion

3.1. Characterization

Fourier-transform infrared spectroscopy (FTIR) analyses were performed to examine the functional groups on the raw SP, raw alginate, and Alg-SP beads in the range of 600 and 4,200 cm^{-1}. In Fig. 1, for raw SP biomass the lipid band at around 1,740 cm^{-1}, the amide I and amide II bands near 1,660 and 1,540 cm^{-1}, and the carbohydrate region around 1,200–900 cm^{-1} are shown. Furthermore, the broad peak around 3,350 cm^{-1} represents O–H and overlapped N–H groups and the peak at 2,950 cm^{-1} is attributed to C–H stretching vibration of raw SP. The characteristic peaks at 3,350; 1,610; 1,450 and 1,025 cm^{-1} represent the stretching of O–H, C–O–O (asymmetric), C–O–O (symmetric), and C–O–C (asymmetric) bonds, respectively for raw alginate beads (Fig. 1). The bands positioned around 1,095; 1,075 and 1,035 cm^{-1} are attributed to deformation vibration of C–C band, stretching vibration of C–O–C, and O–H bending vibration. Several differences appeared in the FTIR spectra of Alg-SP beads in comparison with raw SP and Alg beads (Fig. 1). The peaks near 3,300; 1,550; 1,425 and 1,250 cm^{-1} are assigned to the O–H and N–H (overlap), N–H (amide II), C–O–O (symmetric), and C–O stretching formed by the interaction between raw SP and alginate. According to the FTIR spectrum of Alg-SP beads, a peak at 1,550 cm^{-1} was invisible in the alginate molecular structure and corresponded to secondary amine bending from the protein structure of *Spirulina*. Therefore, an increment in the intensity of the peaks at 2,950 and 1,250 cm^{-1} related to C–H and C–O stretching is evidence for interactions of SP and alginate molecules [9,13].

The X-ray diffraction (XRD) patterns of the samples are presented in Fig. 2. There were two obvious peaks at

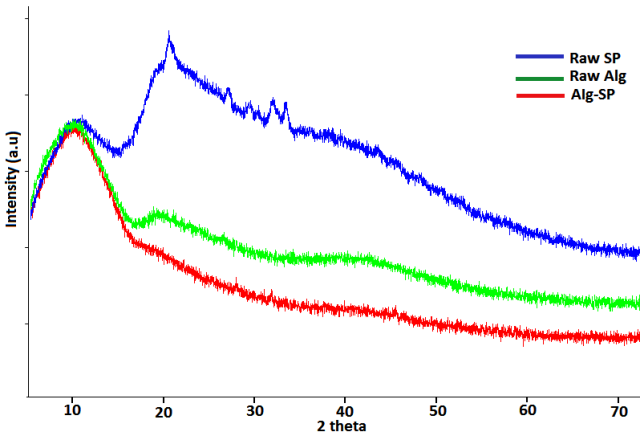

Fig. 2. XRD patterns of raw *Spirulina*, raw alginate, and *Spirulina*-immobilized alginate beads.

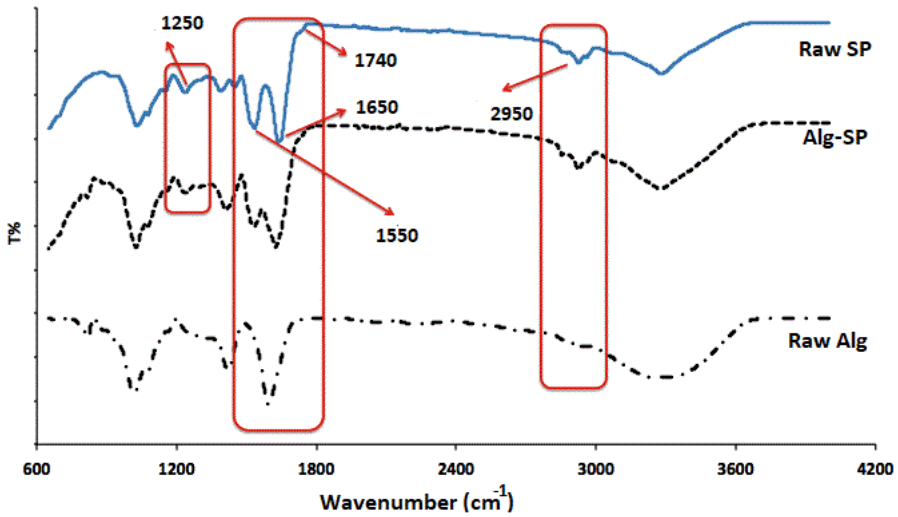

Fig. 1. FTIR spectra of raw *Spirulina*, raw alginate, and *Spirulina*-immobilized alginate beads.

2θ of about 10° and 20° in the XRD pattern of *Spirulina* biomass. These crystal peaks represented crystalline and/or stereo complex crystals in the protein structure of raw SP. These features represent the typical amino acid/protein phase of SP, reflecting the α–helix and β–sheet structures, respectively [17]. The diffraction of raw alginate consisted of three crystalline peaks at 2θ = 13.7°, 23.0°, and 40°. However, alginate X-ray diffraction consists of only two crystalline peaks at 2θ = 13.7° and 23.0° in the literature. This difference may be because of the amounts of guluronic and mannuronic acids present in the different alginate samples. The crystallinity of SP was not observed in the Alg-SP beads due to the strong interaction between alginate and SP. This interaction destroyed the close packing of the alginate molecules required for the formation of regular crystallites. The change in the XRD pattern of the Alg-SP beads is proof the interaction between alginate and SP.

Scanning electron microscopy (SEM) was carried out in order to verify the surface characteristics of raw SP, raw Alg, and Alg-SP-(1.0–3.0) beads (Fig. 3). *Spirulina* biomass presented different forms with 10–50 μm length, 3 μm diameter (low and high magnification, ×1,000 and ×10,000). The inhomogeneous internal structure of raw SP had very small pores and interconnected rooms around the closed cells. The SEM images of raw Alg and Alg-SP-(1.0–3.0) beads are also given in Fig. 3. As can be seen from the figure, there were numerous microfractures (ca. 100–400 μm) on the surface of the raw Alg beads; the fractures covered the entire polymer surface. The surface of the raw beads was full of cracks. These cracks can be characterized as microfractures on the surface of the beads instead of pores. Alg-SP-1.0 beads were found to have lower numbers of shorter microfractures (ca. 50 μm) together with the presence of cracks which were similar to the surface of the raw alginate beads. The low interaction between the SP and alginate molecules may be explained as being associated with the reduction in physical bonds due to low SP content. The decrease in the number of microfractures on the beads with increasing SP content was ascribed to the formation of interactions between the mentioned groups on the SP and alginate molecules. Also, at higher amounts of SP (2% and 3%, w/v), the microfracture structures of the beads were found to be disrupted and had almost completely regular and homogeneous rough surface. This was attributed to relatively more interactions between SP and alginate. When the amount of SP was above 1.0%, a rougher structure with homogeneous surface was obtained. The rough morphologies observed in the Alg-SP-(2.0 and 3.0) beads were explained by the higher amounts of SP leading to additional crosslinks. These physical crosslinks resulted from the electrostatic interactions and hydrogen bonding of the SP and alginate molecules.

The thermal stabilities of raw alginate and Alg-SP beads were characterized by thermogravimetric analysis (Fig. 4). The char yield of Alg-SP beads was determined to be nearly the same as that of raw Alg beads. The char yield ratios were found to be 35%, 35%, and 38% for Alg-SP-(1.0–3.0), respectively. Nearly 60% of the beads decomposed before 400°C and all beads were unstable when temperature increased. In addition, a lower degradation rate was detected for Alg-SP-(2.0 and 3.0) beads in

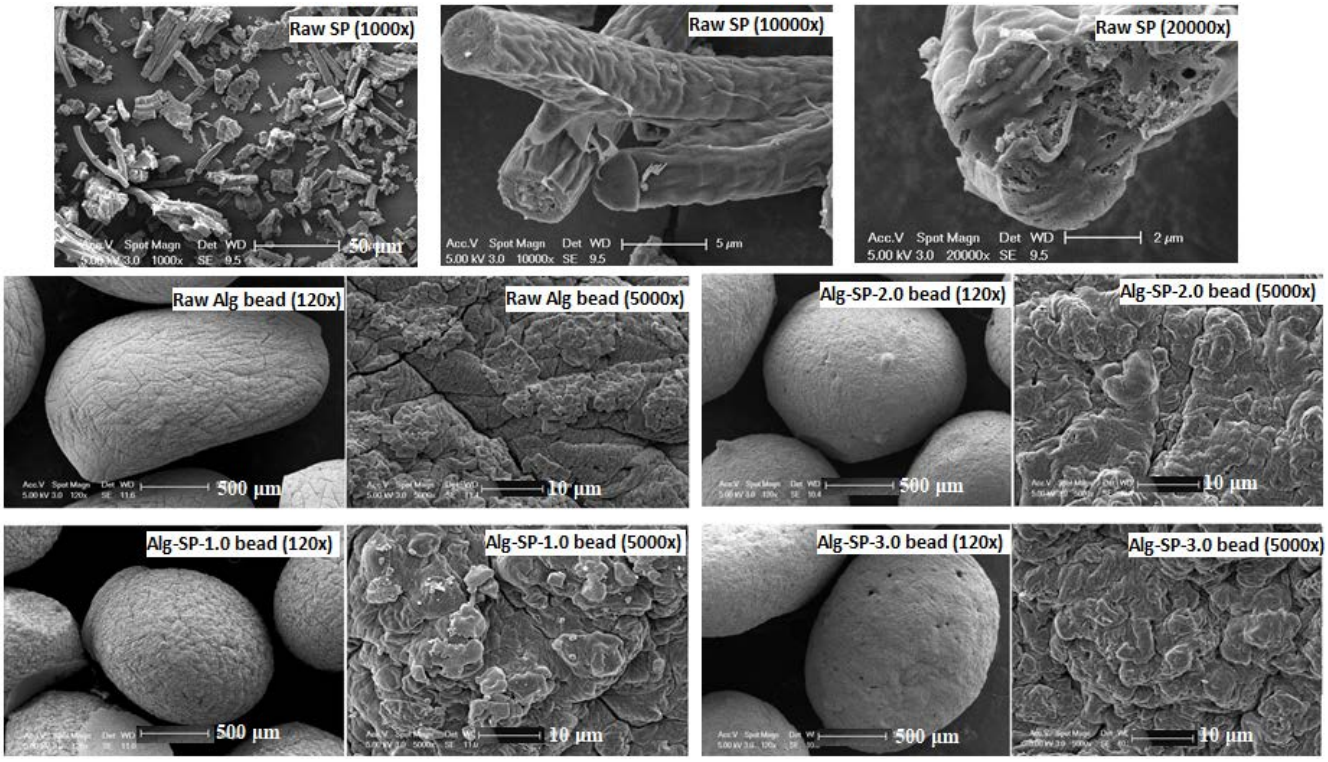

Fig. 3. SEM images of raw *Spirulina* (1000×, 10000×, and 20000×), raw alginate, and *Spirulina*-immobilized alginate beads (×120 and ×5000) magnifications.

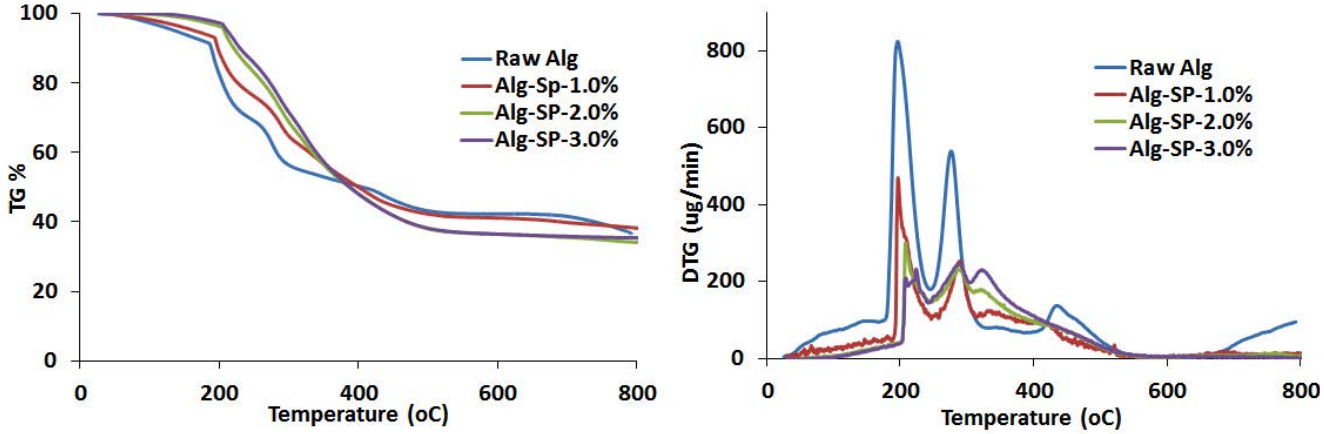

Fig. 4. Thermogravimetric analysis and derivative curves for raw alginate and *Spirulina*-immobilized alginate beads.

the temperature range of 25°C and 400°C. Higher thermal stability with a low degradation rate for the Alg-SP-(2.0 and 3.0) beads was ascribed to the encompassing interaction between Alg and SP. It was observed that the introduction of SP to the Alg molecule decreased the molecular flexibility of the Alg-SP chains. The midpoint degradation temperature decreased with an increasing amount of SP in the alginate. The T_{d50} values were 378°C, 378°C and 401°C as SP content decreased from 3.0 to 1.0% (w/v), respectively. As can be seen from the DTG trace (Fig. 4), raw alginate beads degraded at a faster rate in the temperature range of 25°C–600°C compared with Alg-SP beads. The weight loss was probably due to the removal of water and the degradation of the end-chain groups in the alginate matrix. Three degradation stages were detected at near 200°C, 278°C and 400°C. Moreover, Fig. 4 shows three degradation stages for all Alg-SP beads. End groups in Alg-SP beads degraded above 200°C. The first stage was in the range of 200°C–235°C, the second stage was between 250°C–288°C, and the third part was about 300°C–328°C. In addition, from the comparison of DTG curves, it appeared that the first and second decomposition region resulted from the deterioration of the alginate molecules. Alg-SP beads had a lower degradation rate and moderate degradation temperature compared to raw alginate beads. Furthermore, raw alginate had a 3.7 times higher degradation rate than Alg-SP-3.0. Alg-SP-1.0 had the lowest thermal stability. Thermal stability may be based on the minimized synergy between SP and alginate which then leads to inhibited molecular flexibility of the beads. Consequently, Alg-SP beads had higher thermal stability with the nearly same char yield compared to raw alginate beads. This enhancement in thermal stability was attributed to increases in the interaction between alginate and SP and restriction of the molecular mobility of polymer chains.

DSC analyses of the raw alginate and Alg-SP beads were conducted between –80°C and 350°C under nitrogen atmosphere (Fig. 5). Two endothermic peaks near 80°C–220°C followed by an exothermic peak at nearly 270°C, respectively, appeared for the alginate molecule. The initial endothermic peak at about 120°C was due to removal of adsorbed moisture content associated with hydrophilic

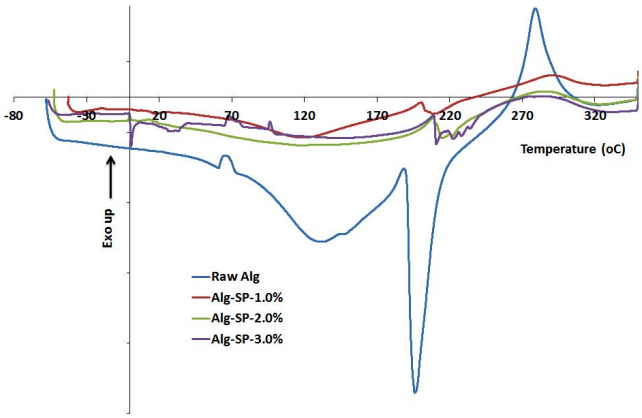

Fig. 5. DSC curves for raw alginate and *Spirulina*-immobilized alginate beads.

groups in the alginate. The sharp endothermic peak appearing at 200°C was related to the melting point of the raw alginate beads. The thermogram of the beads showed a broad exothermic peak after 250°C, which represents its decomposition. In agreement with TG results, these processes were ascribed to carbonized residue because of the decomposition of the polymer. As shown in Fig. 5, Alg-SP-1.0 beads melted at 205°C, which was characterized by an endothermic peak at between 200°C and 226°C. DSC curves of Alg-SP-(2.0 and 3.0) beads had significant differences in the melting region of the raw alginate and Alg-SP-1.0. They showed four different melting peaks at around 210°C and 235°C. This was ascribed to the high content of SP leading to changes in the chain arrangement of the alginate. So, the related peaks were attributed to melting of the polymer crystals in high interactions with *Spirulina*. These four peaks were much more distinct in the DSC thermogram of Alg-SP-3.0 containing the highest amount of SP.

3.2. Preliminary adsorption experiments

Fig. 6a displays the removal percentages of dyes using 100 mg of Alg-SP beads with different SP ratios for

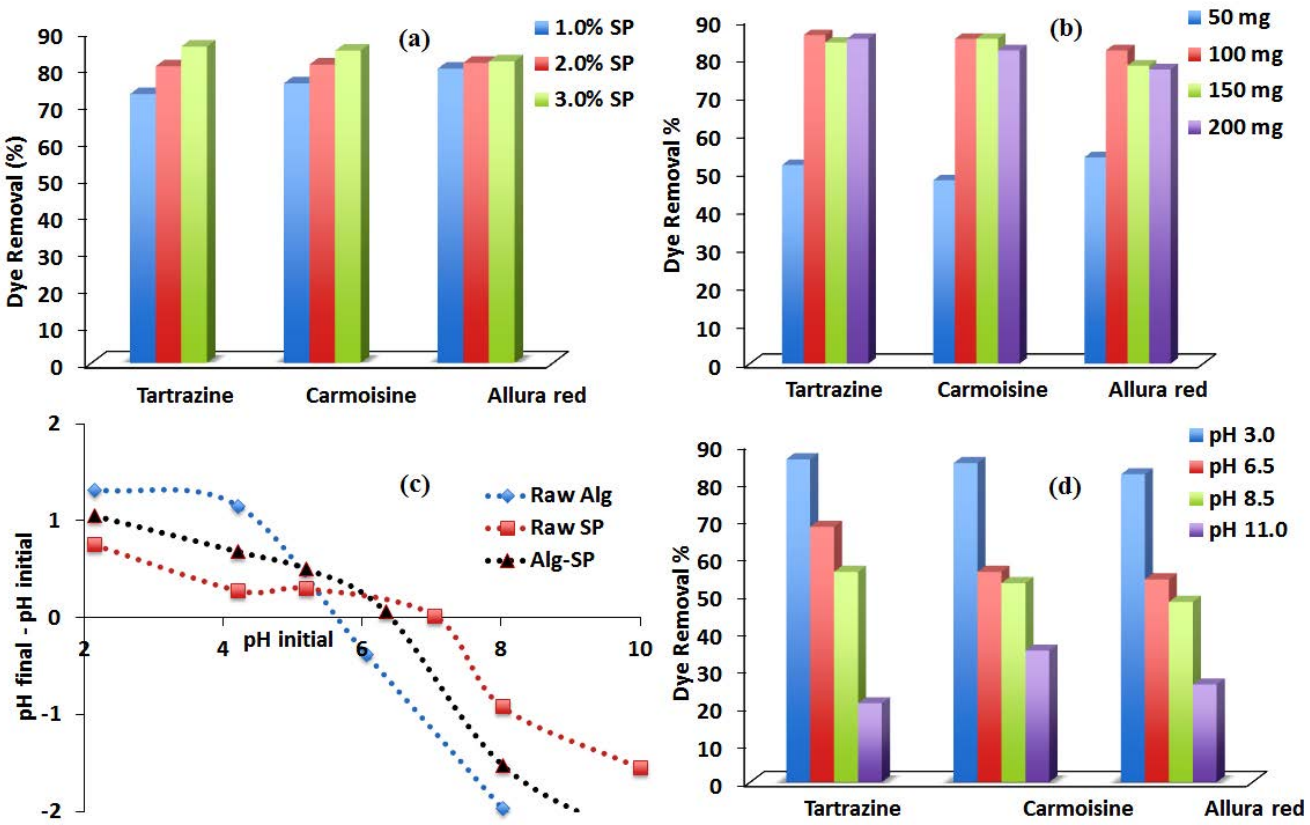

Fig. 6. (a) Effect of SP amount on the removal % of dyes, (b) effect of adsorbent amount on the removal % of dyes, (c) surface charge of raw *Spirulina*, raw alginate and Alg-SP beads, and (d) effect of pH on the removal % of dyes.

50 mg L^{-1} initial dye concentrations within 1 h. Removal % values of tartrazine were detected to be 86%, 80%, and 73%; carmoisine removal % values were determined to be 85%, 81%, and 76%; and Allura Red removal % values were found to be 82%, 81%, and 80% using Alg-SP-3.0, Alg-SP-2.0, and Alg-SP-1.0 beads, respectively. As the SP content ratio increased from 1.0 to 3.0% (w/v), dye adsorption removal percentages were seriously boosted. Thus, 3.0% (w/v) SP content in the alginate beads was used as the optimum SP content for further adsorption experiments.

The effect of amount of adsorbent on dye adsorption was investigated in the range of 50 to 200 mg of Alg-SP-3.0 for 1 h adsorption process as shown in Fig. 6b. The dye removal percentages increased sharply from 52% to 86% for tartrazine; from 48% to 85% for carmoisine; and from 54% to 82% for Allura Red, respectively, as the amount of adsorbent increased from 50 to 100 mg g^{-1}. The increase in dye removal percentage with adsorbent content was attributed to increased adsorbent surface area and availability of active sites. Hence, 100 mg of beads were chosen as the optimum amount of adsorbent and 100 mg of Alg-SP-3.0 was applied to investigate the effect of pH on the dye adsorption experiments.

The PZC of an adsorbent is the pH at which the surface has a net neutral charge. The adsorbent is protonated in solutions with pH less than the PZC, and thus the adsorbent can be adsorb anions; contrarily, it is deprotonated in solutions with pH higher than the PZC, and the adsorbent can adsorb cations [13,18].

The raw Alg beads had positive surface charge at pH lower than 6.0 owing to the presence of –COOH groups in the molecule. PZC for SP and Alg-SP beads were recorded as pH 7.0 and 6.34, respectively (Fig. 6c). When compared with raw Alg, the PZC values of Alg-SP beads increased after embedding SP due to the deprotonated carboxylic acids of alginate.

The pH value of the solution is an important parameter for the adsorption process, and the initial pH value of the dye solutions have significant influence compared to the final pH. In the present study, experiments were carried out in the pH range 3.0–11.0 for 1 h to examine the effect of pH on dye adsorption. The removal % of dyes decreased from 86% to 21%; 85% to 35%; and 82% to 26% for tartrazine, carmoisine, and Allura Red, respectively, when the pH increased from 3.0 to 11.0 (Fig. 6d). In general, initial pH value may enhance or reduce the adsorption. This was attributed to the charge on the adsorbent surface with the change in pH value. Similar behaviours of removal % with pH can be explained by considering the similarity in the structure of the dyes. At pH 3.0, the beads were protonated with –COOH and –OH functional groups; thus, a positive charge was formed on the beads and hydrogen bonds formed between –OH and –COOH groups of the beads and N=N of dyes and adsorption efficiency significantly

increased. At pH 11.0, the –COOH groups on the beads were ionized completely and there was electrostatic repulsion between $–SO_3$ groups on the dyes and adsorption capacity sharply decreased. Therefore, adsorption of dyes onto Alg-SP-3.0 beads may be due to hydrogen bonding, electrostatic repulsion, Van der Waals forces, and other effects.

3.3. Adsorption isotherms

Equilibrium adsorption isotherms for tartrazine, carmoisine, and Allura Red by Alg-SP-3.0 are shown in Fig. 7. The following models defined the relationship between dyes adsorption and the equilibrium concentrations: Langmuir [19], Freundlich [20], D–R, Temkin, Halsey [21], and Harkins–Jura [22]. Isotherm parameters can be obtained from the slope and intercept of the related plots. Fig. 7 and Table 1 represent the adsorption isotherm parameters and correlation coefficients (R^2).

The Langmuir isotherm analyses the surface coverage by counterbalancing the relative rates of adsorption. The adsorption is based on the number of active sites on the adsorbent. In addition, the isotherm assumes monolayer coverage of the adsorbent. The isotherm is defined in Eqs. (1) and (2):

$$\frac{1}{q_e} = \frac{1}{q_m K_L}\frac{1}{C_e} + \frac{1}{q_m} \tag{1}$$

$$R_L = \frac{1}{\left(1 + C_e K_L\right)} \tag{2}$$

where q_e (mg g^{-1}) and C_e (mg L^{-1}) are the amount of adsorbate per unit mass of adsorbent and concentration at equilibrium, respectively. q_m (mg g^{-1}) is the maximum amount of adsorbate per unit mass of adsorbent to form a monolayer on the surface. K_L (mg L^{-1}) is the Langmuir constant related to the affinity of the binding sites. Furthermore, R_L indicates the adsorption is unfavourable when $R_L > 1.0$, favourable when $0 < R_L < 1.0$, and irreversible when $R_L = 0$ [23].

In this study, the linear regression coefficient (R^2) values were found in the range of 0.88 and 0.91, and the isotherm was accepted as fitting the Langmuir isotherm well according to high R^2 values. K_L values were 39.22 L mg^{-1} for tartrazine; 27.00 L mg^{-1} for carmoisine; and 49.27 L mg^{-1} for Allura Red, respectively. R_L values were calculated as 5×10^{-4}, 7×10^{-4} and 4×10^{-4}, for tartrazine, carmoisine, and Allura Red, respectively (Fig. 7 and Table 1). R_L values for all dyes were lower than 1.0, and it was concluded that dye adsorption onto Alg-SP beads was favourable. q_m values were estimated to be 76.92, 50.00, and 71.42 mg g^{-1} for tartrazine, carmoisine, and Allura Red, respectively (Table 1). According to the R^2, R_L and K_L values, the Langmuir model was accepted as suitable for dye adsorption. This confirmed the surface homogeneity of the beads. Moreover, based on the Langmuir isotherm model principle, it can be safely stated that each active site on the beads interacted with only one dye molecule. Dye molecules adsorbed on well-defined localized sites of the beads and the saturation coverage corresponded to complete occupancy of these sites. The adsorption sites on the beads were all energetically homogeneous, and there was no interaction between adjacent dye molecules.

The Freundlich isotherm model is usually applied for non-ideal reversible adsorption processes and it gives information regarding multilayer adsorption with the non-uniform distribution of heat, which takes place on a heterogeneous surface and is expressed in Eq. (3):

$$q_e = K_F C_e^{1/n} \tag{3}$$

In Eq. (3), q_e (mg g^{-1}) and C_e (mg L^{-1}) are the amount of adsorbate per unit mass of adsorbent and concentration at equilibrium, respectively. K_F and $1/n$ are the relative adsorption capacity and the heterogeneity factor of the surface, respectively. The value of $1/n$ illustrates the adsorption to be favourable when $1/n < 1.0$, difficult when $0.5 < 1/n < 1.0$, and unfavourable when $1/n > 1.0$.

In the present paper, K_F and $1/n$ values were calculated as 4.57 mg g^{-1} and 0.53 for tartrazine; 4.36 mg g^{-1} and 0.50 for carmoisine; and 3.16 mg g^{-1} and 0.60 for Allura Red, respectively, as indicated in Table 1. For dye adsorption onto the beads, $1/n$ values were lower than 1.0. Previous research indicated that the value of n greater than 1.0 for all adsorbents showed favourable adsorption [23]. This value should be in the range of 1.0–10.0 for better adsorption. Thus, in the present paper, the adsorption process was not favourable as the calculated values of n were in the range of 1.67 and 2.00. The R^2 values for these dyes varied between 0.73 and 0.80. Low R^2 values were less than for the Langmuir isotherm model, suggesting that the mode of adsorption was not heterogeneous in nature. The Freundlich model did not apply effectively to the adsorption process of dyes using Alg-SP beads.

The D–R isotherm explains an adsorption mechanism with Gaussian energy distribution onto heterogeneous adsorbent surfaces and is expressed as follows:

$$\ln q_e = \ln q_m - \beta\left(\text{epsilon}\right)^2 \tag{4}$$

$$\varepsilon = RT\ln\left(1 + \frac{1}{C_e}\right) \tag{5}$$

$$\text{Energy} = \frac{1}{\sqrt{2\beta}} \tag{6}$$

In Eqs. (4)–(6), q_e (mg g^{-1}) and q_m (mol g^{-1}) are the amount of adsorbate per unit mass of adsorbent and the maximum amount of adsorbate per unit mass of adsorbent, respectively, β (mol² kJ^{-2}) and ε are D–R isotherm constants, R (8.314 J $mol^{-1}K^{-1}$) is gas constant, and T (K) is temperature. The model assumes the pore-filling mechanism and that this behaviour is associated with Van der Waal's bonds and physical adsorption [24].

q_m and β (Table 1) were calculated to be 29.96 mol g^{-1} and 1×10^{-5} mol² kJ^{-2}; 25.28 mol g^{-1} and 1×10^{-5} mol² kJ^{-2}; and 26.84 mol g^{-1} and 1×10^{-5} mol² kJ^{-2} for tartrazine, carmoisine, and Allura Red, respectively. The R^2 values were calculated between 0.89 and 0.94 indicating significant

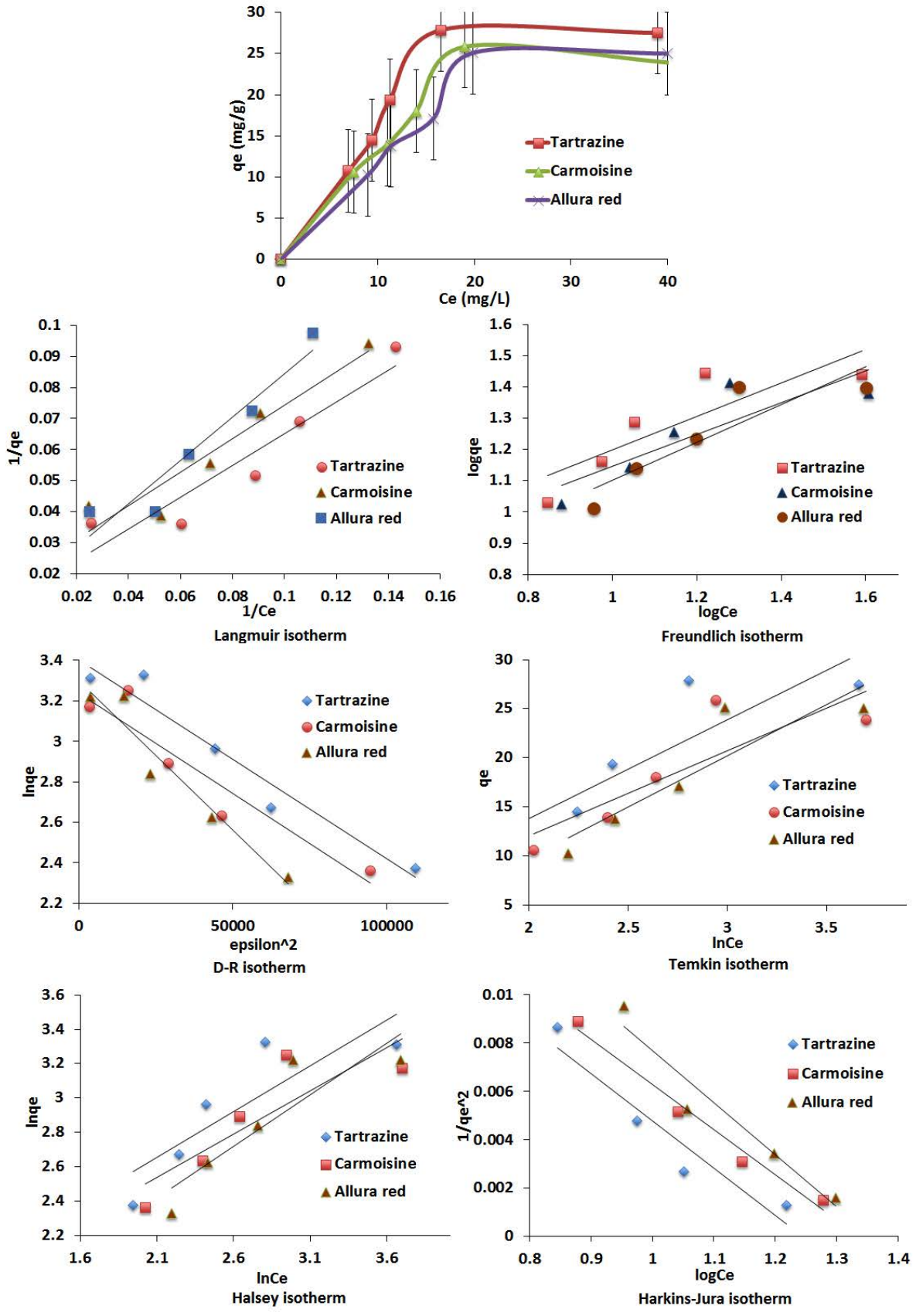

Fig. 7. Adsorption isotherms for dyes onto *Spirulina*-immobilized alginate beads.

Table 1
Adsorption isotherm constants for a dye adsorption onto Alg-SP-3.0 beads

	Tartrazine	Carmoisine	Allura Red
Langmuir isotherm model			
q_m (mg g^{-1})	76.92	50.00	71.42
K_L (L mg^{-1})	39.22	27.00	49.28
R_L	5×10^{-4}	7×10^{-4}	4×10^{-4}
R^2	0.88	0.90	0.91
Freundlich isotherm model			
K_F (mg g^{-1})	4.57	4.36	3.16
$1/n$	0.53	0.50	0.60
R^2	0.73	0.74	0.80
Dubinin–Radushkevich isotherm model			
q_m (mol g^{-1})	29.96	25.28	26.84
β (mol^2 kJ^{-2})	1×10^{-5}	1×10^{-5}	1×10^{-5}
Energy (kJ mol^{-1})	0.22	0.22	0.22
R^2	0.94	0.89	0.93
Temkin isotherm model			
K_t (L g^{-1})	0.53	0.54	0.34
b (kJ mol^{-1})	0.24	0.28	0.23
R^2	0.76	0.73	0.81
Halsey isotherm model			
n_H	0.53	0.50	0.60
K_H (mg g^{-1})	2.25	2.10	1.99
R^2	0.73	0.74	0.80
Harkins–Jura isotherm model			
A (g mg^{-1})	51.02	53.47	46.29
B (mg g^{-1})	1.22	1.33	1.34
R^2	0.90	0.97	0.93

fit. An adsorption process is called physical if the energy is lower than 8 kJ mol^{-1} and it is called chemisorption if the energy values are between 8.0 and 16.0 kJ mol^{-1} [24]. The mean free energies were calculated to be 0.22 kJ mol^{-1} for all dyes (Table 1) and the energy corresponded with the mechanism of dye adsorption onto beads, which was a physical adsorption process.

The Temkin isotherm accepts linear decreases in adsorption heat while the adsorbent active sites are covered by adsorbate, the adsorption is characterized by a uniform distribution of binding energies of the adsorbate, and the isotherm assumes adsorbate–adsorbent interaction [13,21].

$$q_e = \frac{RT\ln\left(K_t C_e\right)}{b} \tag{7}$$

Eq. (7) expresses the Temkin isotherm with K_t (L g^{-1}) being the Temkin isotherm equilibrium binding constant, b (J mol^{-1}) the heat of adsorption constant, R (8.314 J mol^{-1} K^{-1}) is the universal gas constant and T (K) is temperature.

As shown in Table 1, K_t values were determined to be 0.53, 0.54, and 0.34 L g^{-1} for tartrazine, carmoisine, and Allura Red, respectively. Also, the heat of adsorption (b) values decreased from 0.28 (for carmoisine) to 0.23 kJ mol^{-1} (for Allura Red). The adsorption heat was calculated between 0.23 and 0.28 kJ mol^{-1} for all dyes. Based on the R^2 values, it was concluded that the Temkin model fitted the equilibrium data well. The high R^2 values showed that the heat of the adsorption of dye molecules in a layer decreased with the surface coverage of the dye-Alg-SP-3.0 bead interaction.

The Halsey isotherm considers multilayer adsorption onto a heterogeneous adsorbent surface and is defined by Eq. (8).

$$q_e = \frac{1}{n_H}\ln K_H - \frac{1}{n_H}\ln C_e \tag{8}$$

where K_H and n_H are Halsey isotherm constants [21].

The Halsey isotherm was used to study the sorption energy of multilayers of dye adsorbed on the surface of the beads. Values of R^2 (in the range of 0.73 and 0.80) indicated the applicability of Halsey adsorption isotherm but the model was less applicable compared to the Langmuir and Harkins–Jura adsorption isotherms.

The Harkins–Jura isotherm assumes multilayer adsorption occurring on an adsorbent surface with a heterogeneous pore distribution [9,22].

$$\frac{1}{q_e^2} = \frac{B}{A} - \left(\frac{1}{A}\right)\log C_e \tag{9}$$

In Eq. (9), A and B are Harkins–Jura constants.

The values of constants A and B in the isotherm were calculated to be 51.02 g mg^{-1} and 1.22 mg g^{-1}; 53.47 g mg^{-1} and 1.33 mg g^{-1}; and 46.29 g mg^{-1} and 1.34 mg g^{-1} for tartrazine, carmoisine, and Allura Red, respectively (Table 1). This model showed better fit to the adsorption data with R^2 values in the range of 0.90 and 0.97. Values of R^2 for this isotherm indicate that the adsorption process for dyes on the bead surface was best explained by the Harkin Jura adsorption isotherm.

Notice that, it can be concluded that the Langmuir, D–R, Temkin and Harkins–Jura isotherm models had much better fit than the Freundlich and Halsey models by comparing the values of R^2 of the examined six isotherm models. Therefore, it was evident from the present study that dye molecules were adsorbed onto the Alg-SP beads in accordance with monolayer adsorption and do not permit transmigration of the adsorbate in the plane of the surface.

3.4. Adsorption kinetics

Effect of time on the dye adsorption is exhibited in Fig. 8. In general, dye removal using Alg-SP-3.0 beads was quite fast during the first 30 min, then continued at a slow adsorption rate and reached equilibrium at the end of 80 min. Tartrazine and carmoisine adsorption processes reached equilibrium at the end of 80 min. C_e values were determined as nearly 2.0 and 4.5 mg L^{-1} and q_t values were measured to be 12.0 and 11.37 mg g^{-1} for tartrazine and

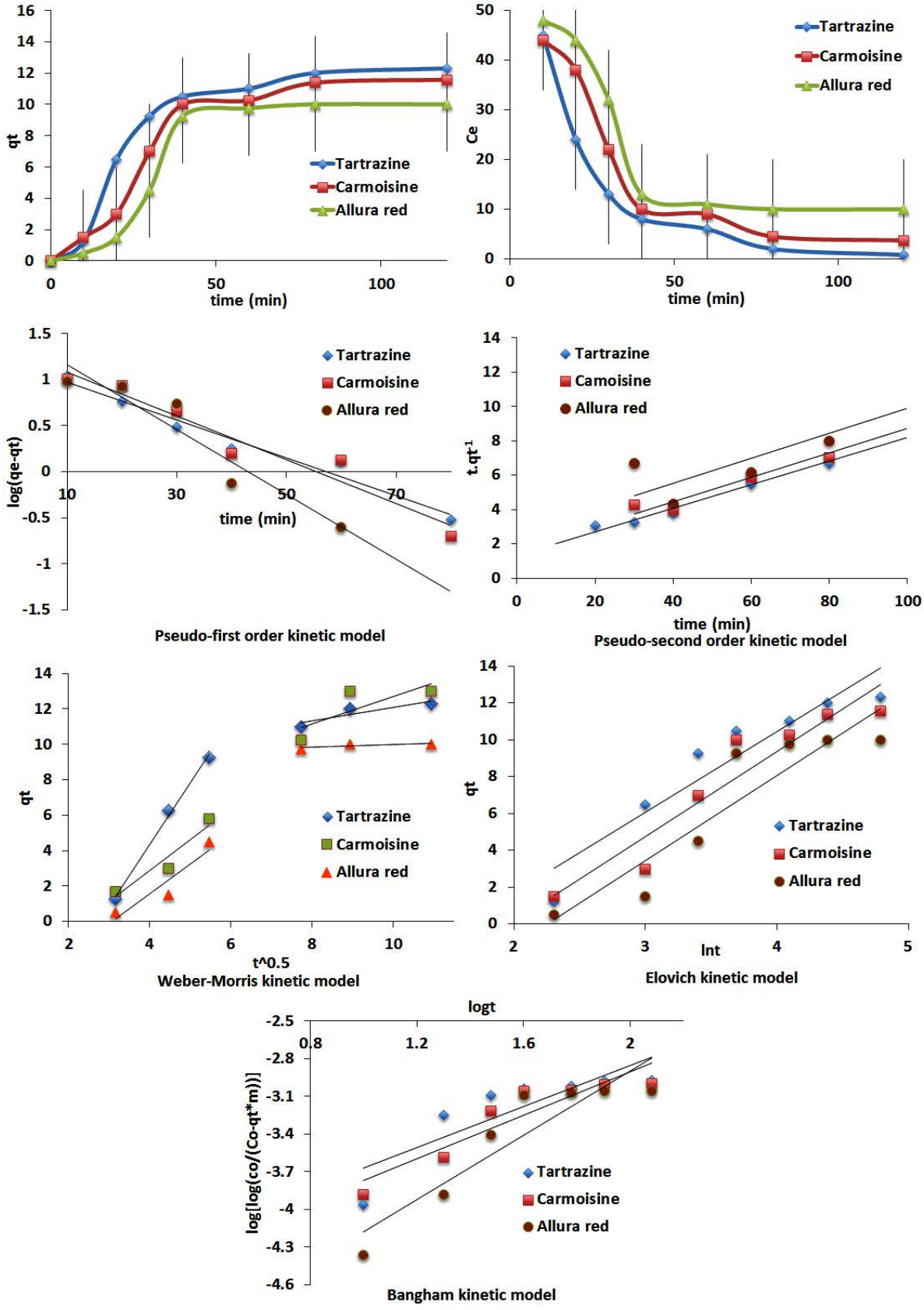

Fig. 8. Adsorption kinetics for dyes onto *Spirulina*-immobilized alginate beads.

carmoisine, respectively. Furthermore, Allura Red adsorption onto Alg-SP-3.0 beads reached equilibrium at the end of 40 min. C_e and q_t values were determined to be nearly 13.0 mg L^{-1} and 9.25 mg g^{-1}, respectively. For tartrazine and carmoisine removal % values were nearly 88% and 82% after 80 min, while Allura Red had 80% removal percentage at the same time. In addition, tartrazine and carmoisine had 98% and 92% removal after 2 h and Allura Red removal % remained constant after 1 h.

The adsorption kinetics were described using pseudo-first-order, pseudo-second-order [25], Weber–Morris, Elovich, and Bangham [26] models.

The pseudo-first order model can be used for the adsorption of a solid/liquid system and the linearized form is given by Eq. (10).

$$\log\left(q_e - q_t\right) = \log q_e - \frac{k_1}{2.303}t \tag{10}$$

where q_e (mg g^{-1}) and q_t (mg g^{-1}) are the amount of adsorbate per unit mass of adsorbent and at time t, respectively, and k_1 (min^{-1}) is the rate constant for the pseudo-first-order model. The plot of $\ln(q_e - q_t)$ vs. time (min) was drawn and rate constant k_1 (min^{-1}) was calculated as the model constant (Fig. 8 and Table 2) [9,25].

For the pseudo-first-order kinetic, the experimental $q_{e,\text{experimental}}$ values were found as 12.3, 11.6 and 10.0 mg g^{-1} for tartrazine, carmoisine, and Allura Red, respectively. The $q_{e,\text{calculated}}$ values were found to be 15.1, 32.2 and 20.9 mg g^{-1} from the model for the same dyes, and the R^2 values changed between 0.90 and 0.96. According to the data, $q_{e,\text{calculated}}$ values determined were quite different from $q_{e,\text{experimental}}$ values, demonstrating the pseudo-first-order kinetic was not convenient for describing the dye adsorption.

The pseudo-second-order kinetic model [13,25] considers the rate-determining step of the chemical reaction and is expressed by Eq. (11):

$$\frac{t}{q_t} = \frac{1}{k_2 q_e^2} + \frac{1}{q_e}t \tag{11}$$

where k_2 (g mg^{-1} min^{-1}) is pseudo-second-order model constant and $h = k_2 q_e^2$ (mg g^{-1} min^{-1}) is initial sorption rate. From Eq. (11), the plot of t/q_t against time (min) was drawn (Fig. 8) and kinetic parameters were calculated from slope and intercept and k_2 (g mg^{-1} min^{-1}) and initial adsorption rate h (mg g^{-1} min^{-1}) were calculated (Table 2).

For the pseudo-second-order kinetic, the experimental q_e values were not far from the calculated ones, with values of $q_{e,\text{experimental}}$ = 12.3 mg g^{-1} and $q_{e,\text{calculated}}$ = 14.4 mg g^{-1} for tartrazine; $q_{e,\text{experimental}}$ = 11.6 mg g^{-1} and $q_{e,\text{calculated}}$ = 13.8 mg g^{-1} for carmoisine; $q_{e,\text{experimental}}$ = 10.0 mg g^{-1} and $q_{e,\text{calculated}}$ = 12.5 mg g^{-1} for Allura Red. The adsorption rate constants, h, were calculated as 0.76, 0.36 and 0.62 mg g^{-1} min^{-1} for tartrazine, carmoisine, and Allura Red, respectively. R^2 values changed in the range of 0.81 and 0.99. These results indicate that the dye adsorption onto Alg-SP-3.0 beads was explained better by the pseudo-second-order kinetics than other kinetic models.

The Weber–Morris intra-particle diffusion model with multi-linearity correlation explains the mass transfer phenomena of the adsorption and the model is defined by Eq. (12):

$$q_t = k_{\text{id}} t^{0.5} + C \tag{12}$$

where k_{id} (mg g^{-1} $min^{-0.5}$) is the intraparticle rate constant. The q_t vs. $t^{0.5}$ graph was plotted from Eq. (12) and k_{id1} (mg g^{-1} $min^{-0.5}$) and k_{id2} values were calculated from the slope of the plot (Fig. 8 and Table 2).

In this paper, the R^2 values for Weber–Morris intraparticle diffusion were calculated in the range of 0.87–0.99 and also 0.61–0.80. From Fig. 8, two separate linear phases with different slope were determined, which was explained as the occurrence of different mass transfer phenomena. The first phase in first 30 min indicated the boundary layer mass transfer and diffusion phenomena through the external surface of the beads [26]. The second linear part between 40 and 120 min describes intraparticle mass transfer. According to Table 2, k_{id1} and k_{id2} for tartrazine, carmoisine, and Allura Red established that intraparticle mass transfer rates were slower than the boundary layer mass transfer rate. Also, k_{id1} and k_{id2} constants for Allura Red, tartrazine and carmoisine were calculated as k_{id1} = 1.68 mg g^{-1} $min^{-0.5}$ and k_{id2} = 0.07 mg g^{-1} $min^{-0.5}$; k_{id1} = 3.47 mg g^{-1} $min^{-0.5}$ and

Table 2
Kinetic constants of dye adsorption onto Alg-SP-3.0 beads

	Tartrazine	Carmoisine	Allura Red
$q_{e,\text{experimental}}$ (mg g^{-1})	12.3	11.6	10.0
Pseudo-first-order kinetic model			
$q_{e,\text{calculated}}$ (mg g^{-1})	15.1	32.2	20.9
k_1 (min^{-1})	0.047	0.080	0.054
R^2	0.96	0.90	0.94
Pseudo-second-order kinetic model			
$q_{e,\text{calculated}}$ (mg g^{-1})	14.4	13.8	12.5
k_2 (g mg^{-1} min^{-1})	3.65×10^{-3}	1.95×10^{-3}	1.82×10^{-3}
h (mg g^{-1} min^{-1})	0.76	0.36	0.62
R^2	0.99	0.81	0.97
Weber–Morris intra-particle diffusion kinetic model			
k_{id1} (mg g^{-1} $min^{-0.5}$)	3.47	1.73	1.68
R^2	0.99	0.92	0.87
k_{id2} (mg g^{-1} $min^{-0.5}$)	0.37	0.74	0.07
R^2	0.81	0.77	0.61
Elovich kinetic model			
β (g mg^{-1})	0.23	0.22	0.22
α (mg g^{-1} min^{-1})	0.87	0.63	0.48
R^2	0.89	0.90	0.95
Bangham kinetic model			
k_0 (L g^{-1})	1.86×10^{-4}	1.35×10^{-4}	2.04×10^{-5}
α	0.82	0.86	1.28
R^2	0.73	0.85	0.84

k_{id2} = 0.37 mg g^{-1} min$^{-0.5}$; and k_{id1} = 1.73 mg g^{-1} min$^{-0.5}$ and k_{id2} = 0.74 mg g^{-1} min$^{-0.5}$, respectively. These results describe the boundary layer mass transfer rate as twenty-four-fold, ten-fold and three-fold the interior mass transfer rate for Allura Red, tartrazine and carmoisine, respectively.

The Elovich model explains heterogeneous systems for chemical sorption. The linearized form of the model is expressed Eq. (13):

$$q_t = \frac{1}{\beta}\ln(\alpha\beta) + \frac{1}{\beta}\ln t \tag{13}$$

In Eq. (13), β (g mg^{-1}) is the adsorbent activation energy of chemical sorption and α (mg g^{-1} min^{-1}) is the initial velocity. The plots of q_t against ln$t$ for Elovich's model are presented in Fig. 8. α (mg g^{-1} min^{-1}) and β (g mg^{-1}) values represent the adsorption rate constant and the number of available sites for adsorption, respectively, and were calculated from the slope and intercept of the plot (Table 2) [13,26].

The correlation coefficients (R^2) for the Elovich model were determined in the range of 0.89 and 0.95 and the initial adsorption rate (α) values were determined to be $\alpha_{tartrazine}$ = 0.87 mg g^{-1} min^{-1}, $\alpha_{carmoisine}$ = 0.63 mg g^{-1} min^{-1}, and $\alpha_{Allura\ Red}$ = 0.48 mg g^{-1} min^{-1}. It can be safely stated that Elovich's model fitted the dye adsorption sufficiently.

The Bangham model assumes that pore diffusion controls the adsorption rate [9] and is expressed by Eq. (14).

$$\log\left[\log\left(\frac{C_0}{C_0 - q_t m}\right)\right] = \log\left(\frac{k_0 m}{2.303V}\right) + \alpha\log t \tag{14}$$

where k_0 (L g^{-1}) and α are Bangham model constants [26].

The R^2 values were defined in the range of 0.73 and 0.85 for the Bangham model, so pore diffusion played a role during dye adsorption.

3.5. Thermodynamics

Adsorption thermodynamic experiments were carried out at 25°C, 45°C and 60°C at pH 3.0, all dye concentrations were 50 mg L^{-1} and contact time was 1 h. The thermodynamic parameters were calculated from the following equations:

$$\ln\left(\frac{q_e}{C_e}\right) = \frac{\Delta S°}{2.303R} - \frac{\Delta H°}{2.303RT} \tag{15}$$

$$\Delta G° = \Delta H° - T\Delta S° \tag{16}$$

where R is gas constant (8.314 J mol^{-1} K^{-1}) and T is the absolute temperature (K).

In the present study, ΔH° values of tartrazine, carmoisine, and Allura Red adsorption were calculated to be 92.7, 80.5, and 111.2 kJ mol^{-1}, respectively and this indicates that the dye adsorption onto Alg-SP-3.0 beads was endothermic in nature [27]. The endothermic behaviour of dye adsorption was confirmed by the positive values for enthalpy and positive/negative enthalpy values classify chemical or physical adsorption (for chemical adsorption, ΔH° > 35 kJ mol^{-1} and for physical adsorption ΔH° < 35 kJ mol^{-1}). According to Table 3, the positive ΔH° values indicated dye adsorption onto Alg-SP-3.0 beads were endothermic reactions so an increase in temperature supported the adsorption reaction. ΔS° values were determined to be 316, 274 and 383 J mol^{-1} K^{-1} for tartrazine, carmoisine, and Allura Red, respectively, and the positive ΔS° values demonstrated that the disorderliness and conformational entropies of the beads and dye interface increased during the adsorption process.

The adsorption of all dyes by Alg-SP-3.0 beads was spontaneous with negative values for Gibbs free energy. The negative ΔG° values indicate that dye adsorption was a spontaneous process and declined significantly with an increment in temperature showing that spontaneous behaviour of dye removal process onto Alg-SP-3.0 beads changed inversely with temperature. For the defined three temperatures, negative Gibbs free energy values showed that Alg-SP-3.0 beads spontaneously adsorbed dyes.

3.6. Adsorption mechanism

The FTIR spectra of dye and Alg-SP before and after dye adsorption are shown in Fig. 9. The peaks at 3,300; 2,950; 1,550; 1,425 and 1,250 cm^{-1} are attributed to the O–H and N–H (overlaps), C–H, N–H, –COO–, and C–O stretching of the beads, respectively. The dye showed a broad band near 3,400 cm^{-1} attributed to the N–H and O–H stretching. In addition, the peaks at 1,570; 1,500 and 1,350 cm^{-1} correspond to C=C (aromatic rings), N=N and –S=O stretching vibration, respectively. Prominent differences were obtained after the dye adsorption process. The absorption band near 3,300 cm^{-1}, corresponding to the stretching vibration of O–H and N–H, increased on Alg-SP-3.0 after adsorption. This indicates hydrogen bond formation between the hydroxyl groups on the bead and the amine group on the dye molecules. Moreover, the spectra of the beads before and after dye adsorption indicated the absorption band at 1,350 cm^{-1}, corresponding to –SO_3 group, strengthened after adsorption. Wang and Wang [28] also

Table 3
Thermodynamic parameters of dye adsorption onto Alg-SP-3.0 beads

Dye	ΔH° (kJ mol^{-1})	ΔS° (J mol^{-1}K^{-1})	ΔG° (kJ mol^{-1})		
			25°C	45°C	60°C
Tartrazine	92.7	316	–1.46	–7.78	–12.52
Carmoisine	80.5	274	–1.15	–6.63	–10.74
Allura Red	111.2	383	–2.93	–4.59	–10.33

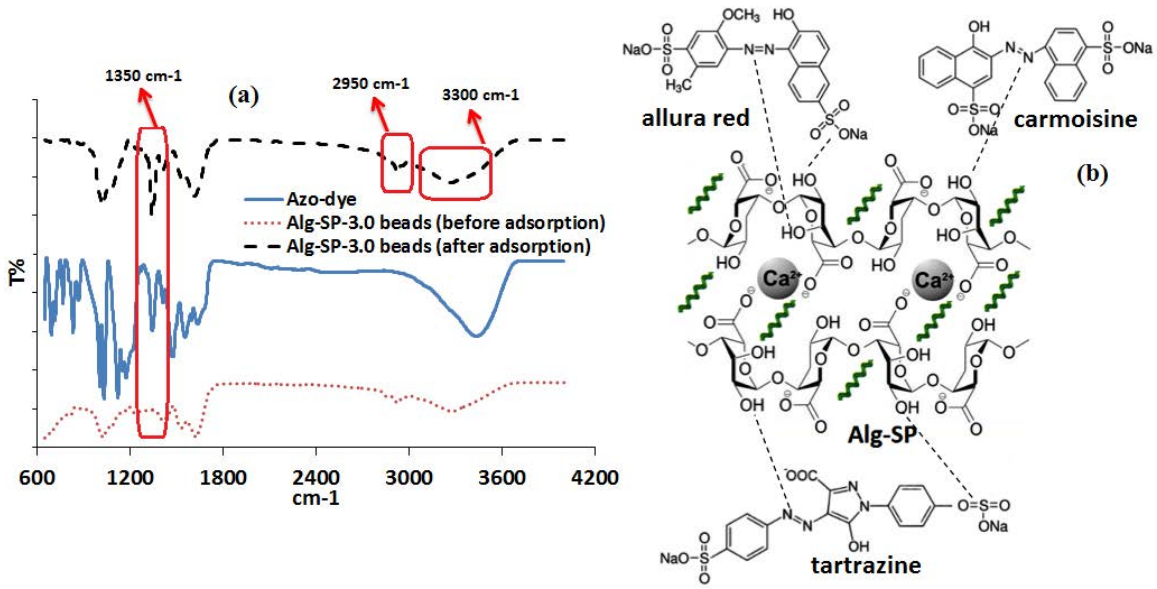

Fig. 9. (a) FTIR spectra of dyes and Alg-SP before and after dye adsorption and (b) possible interactions between Alg-SP-3.0 and dyes.

reported that $–NH_2$, –N=N– and $–SO_3$ groups on dyes were involved in the adsorption process (Fig. 9) [9,14].

3.7. Desorption and reusability

In desorption studies, distilled water at different pH values (pH 3.0, 7.0 and 12.0) were used as eluents to desorb dyes from dye-loaded Alg-SP-3.0 beads. When the pH value changed from 3.0 to 12.0, desorption efficiency values increased from 4% to 48% for tartrazine; 12% to 36% for carmoisine; and 7% to 52% for Allura Red. This might be due to the increment in the number of negatively charged sites at alkaline pH values which increased the electrostatic repulsion and desorption ratios of the dyes (Fig. 10a).

According to Fig. 10b, NaOH solution was the most efficient medium (84%, 77% and 80% for tartrazine, carmoisine, and Allura Red loaded Alg-SP-3.0 beads, respectively) despite HCl solution being inefficient to desorb the dyes. Therefore, dye adsorption was performed at pH 3.0 and desorption was conducted at pH 12.0, since alkaline conditions did not favour adsorption as discussed in the dye adsorption section about the effect of pH.

Alg-SP-3.0 beads were examined for adsorption capacity in terms of reusability for consecutive 5 cycles. Almost 85% desorption efficiency was achieved using 1.0 M NaOH in the first cycle for all dyes. Alg-SP-3.0 beads showed very high performance in three consecutive cycles with almost 75%–80% adsorption and a loss of 5%–8% dye during stripping. Alg-SP-3.0 beads adsorbed nearly 60% dye even in the fifth cycle (Fig. 10c). Though the dye removal values remained nearly constant for 3 cycles, noticeable decreases occurred after the third cycle, suggesting high capability of the beads during adsorption–desorption processes [9,13].

Alg-SP-3.0 beads were compared to other organic/inorganic adsorbents reported in the literature [29–35] (Table 4). The results showed that Alg-SP-3.0 beads had higher removal % for various dyes and that the unique molecular structure of Alg-SP increased adsorption ability. Alg-SP beads can effectively remove dyes from wastewater in acidic pH ranges.

Table 4
Comparison of dyes with different adsorbents

Dye	Adsorbent	Removal %	References
Congo Red	Cellulose/chitosan	95%	[29]
Tartrazine	Coconut husk	92%	[30]
Tartrazine	Activated red mud	84%	[31]
Methylene blue	Activated carbon	40%	[32]
Rhodamine B	Perlite	86%	[33]
Methylene blue	Iron based metal organic framework	95%	[34]
Congo Red	Guar gum/activated carbon nanocomposite	78%	[35]
Tartrazine	SP immobilized alginate	86%	This study
Carmoisine	SP immobilized alginate	85%	This study
Allura Red	SP immobilized alginate	82%	This study

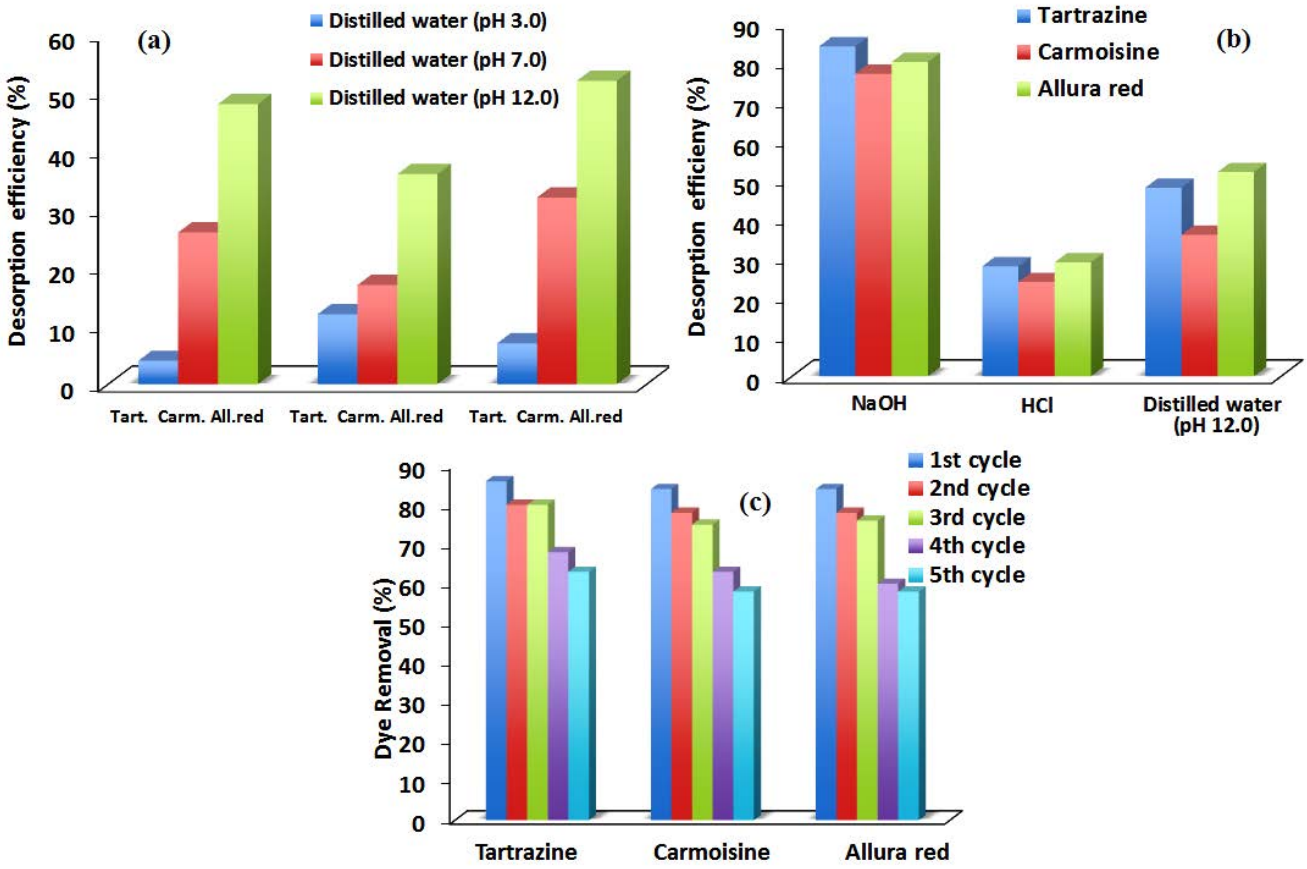

Fig. 10. (a) Desorption and (b) reusability result for dye adsorption onto *Spirulina*-immobilized alginate beads.

4. Conclusions

In summary, the promising adsorbent of *Spirulina*-immobilized alginate beads were synthesized via exchange of monovalent and divalent ions. The beads showed high adsorption capacities for azo-dye tartrazine, carmoisine, and Allura Red, with removal % reaching 86%, 85%, and 82% after 1 h and 98%, 93%, and 82% after 2 h, respectively. Adsorption isotherm and kinetic data of dyes on *Spirulina*-immobilized alginate beads fitted well to the Langmuir and Harkins–Jura isotherm models and pseudo-second-order and Elovich kinetic models, respectively. *Spirulina*-immobilized alginate beads offer an environmentally friendly adsorbent option for dyes. They were clearly observed to have promising potential for the biological treatment of dye-polluted water compared with other adsorbents.

Acknowledgements

This research did not receive any specific grant from funding agencies in the public, commercial, or not-for-profit sectors. The dyes used in this paper were provided by a grant from OMS Gida Group-Mossa.

References

[1] T.W. Seow, C.K. Lim, Removal of dye by adsorption: a review, Int. J. Appl. Eng. Res., 11 (2016) 2675–2679.
[2] M.T. Yagub, T.K. Sen, S. Afroze, H.M. Ang, Dye and its removal from aqueous solution by adsorption: a review, Adv. Colloid Interface Sci., 209 (2014) 172–184.
[3] S. Banerjee, M.C. Chattopadhyaya, Adsorption characteristics for the removal of a toxic dye, tartrazine from aqueous solutions by a low cost agricultural by-product, Arabian J. Chem., 10 (2017) 1629–1638.
[4] I. Balta, B. Sevastre, V. Mireşan, M. Taulescu, C. Raducu, A.L. Longodor, Z. Marchiş, C.S. Mariş, A. Coroian, Protective effect of blackthorn fruits (*Prunus spinosa*) against tartrazine toxicity development in albino Wistar rats, BMC Chem., 13 (2019) 104–115.
[5] I.S. Khan, N. Ali, R. Hamid, S.A. Ganie, Genotoxic effect of two commonly used food dyes metanil yellow and carmoisine using *Allium cepa* L. as indicator, Toxicol. Rep., 7 (2020) 370–375.
[6] A. Gičević, L. Hindija, A. Karačić, Toxicity of Azo Dyes in Pharmaceutical Industry, A. Badnjevic, R. Škrbić, L. Gurbeta Pokvić, Eds., International Conference on Medical and Biological Engineering, IFMBE Proceedings, Vol. 73, Springer, Cham, 2020, pp. 581–587, https://doi.org/10.1007/978-3-030-17971-7_88.
[7] A. Salehi, E.N. Kani, Green cylindrical mesoporous adsorbent based on alkali-activated phosphorous slag: synthesis, dye removal, and RSM modeling, Adsorption, 24 (2018) 647–666.
[8] G.L. Dotto, T.R.S. Cadaval, L.A.A. Pinto, Use of *Spirulina platensis* micro and nanoparticles for the removal synthetic dyes from aqueous solutions by biosorption, Process Biochem., 47 (2012) 1335–1343.
[9] F. Korkut, D. Saloglu, Synthesis, characterization and tetracycline adsorption behaviour of activated carbon doped alginate beads: isotherms, kinetics, thermodynamic and adsorption mechanism, Desal. Water Treat., 206 (2020) 315–330.

[10] J.A.V. Costa, L. Maria Colla, P.F. Duarte Filho, Improving *Spirulina platensis* biomass yield using a fed-batch process, Bioresour. Technol., 92 (2004) 237–241.
[11] M. Nicoletti, Microalgae nutraceuticals, Food, 5 (2016) 54–62, doi: 10.3390/foods5030054.
[12] G.L. Dotto, J.O. Gonçalves, T.R.S. Cadaval Jr., L.A.A. Pinto, Biosorption of phenol onto bionanoparticles from *Spirulina* sp. LEB 18, J. Colloid Interface Sci., 407 (2013) 450–456.
[13] D. Saloglu, N. Ozcan, Activated carbon embedded chitosan/polyvinyl alcohol biocomposites for adsorption of nonsteroidal anti-inflammatory drug-naproxen from wastewater, Desal. Water Treat., 107 (2018) 72–84.
[14] E. Bilgin Simsek, D. Saloglu, N. Ozcan, I. Novak, D. Berek, Carbon fiber embedded chitosan/PVA composites for decontamination of endocrine disruptor bisphenol-A from water, J. Taiwan Inst. Chem. Eng., 70 (2017) 291–301.
[15] L. Liu, S.S. Fan, Y. Li, Removal behavior of Methylene blue from aqueous solution by tea waste: kinetics, isotherms and mechanism, Int. J. Environ. Res. Public Health, 15 (2018) 1321–1337.
[16] T.V. Rêgo, T.R.S. Cadaval Jr., G.L. Dotto, L.A.A. Pinto, Statistical optimization, interaction analysis and desorption studies for the azo dyes adsorption onto chitosan films, J. Colloid Interface Sci., 411 (2013) 27–33.
[17] Y.X. Luo, A. Lode, C.T. Wu, J. Chang, M. Gelinsky, Alginate/nanohydroxyapatite scaffolds with designed core/shell structures fabricated by 3D plotting and in situ mineralization for bone tissue engineering, ACS Appl. Mater. Interfaces, 7 (2015) 6541–6549.
[18] M. Mushtaq, I.M. Tan, L. Ismail, M. Nadeem, M. Sagir, R. Azam, R. Hashmet, Influence of PZC (point of zero charge) on the static adsorption of anionic surfactants on a Malaysian sandstone, J. Dispersion Sci. Technol., 35 (2014) 343–349.
[19] F. Amin, F.N. Talpur, A. Balouch, M.A. Surhio, M.A. Bhutto, Biosorption of fluoride from aqueous solution by white—rot fungus *Pleurotus eryngii* ATCC 90888, Environ. Nanotechnol. Monit. Manage., 3 (2015) 30–37.
[20] H.L. Cai, P.C. Li, Z.X. Ge, Y.X. Xian, D.T. Lu, A new method to determine varying adsorbed density based on Gibbs isotherm of supercritical gas adsorption, Adsorpt. Sci. Technol., 36 (2018) 1687–1699.
[21] Z. Al-Qodah, M. Al-Shannag, Heavy metal ions removal from wastewater using electrocoagulation processes: a comprehensive review, Sep. Sci. Technol., 52 (2017) 2649–2676.
[22] S.-S. Liu, C.-K. Lee, H.-C. Chen, C.-C. Wang, L.-C. Juang, Application of titanate nanotubes for Cu(II) ions adsorptive removal from aqueous solution, Chem. Eng. J., 147 (2009) 188–193.
[23] W.F. Liu, J. Zhang, C.L. Zhang, Y.F. Wang, Y. Li, Adsorptive removal of Cr(VI) by Fe-modified activated carbon prepared from *Trapa natans* husk, Chem. Eng. J., 162 (2010) 677–684.
[24] R. Nadeem, M.A. Naqvi, M.H. Nasir, R. Saeed, T. Iqbal, M. Ashraf, T.M. Ansari, Efficiency of physically pre-treated *Mangifera indica* biomass for Cu^{2+} and Zn^{2+} sequestration, J. Saudi Chem. Soc., 19 (2015) 23–35.
[25] S. Rengaraj, J.-W. Yeon, Y.H. Kim, Y.J. Jung, Y.-K. Ha, W.-H. Kim, Adsorption characteristics of Cu(II) onto ion exchange resins 252H and 1500H: kinetics, isotherms and error analysis, J. Hazard. Mater., 143 (2007) 469–477.
[26] P. Mondal, B. Mohanty, C.B. Majumder, Removal of arsenic from simulated groundwater using GAC-Ca in batch reactor: kinetics and equilibrium studies, Clean–Soil Air Water., 40 (2012) 506–514.
[27] S. Vasudevan, J. Lakshmi, Effects of alternating and direct current in electrocoagulation process on the removal of cadmium from water – a novel approach, Sep. Sci. Technol., 80 (2011) 643–651.
[28] R.Z. Wang, Q.B. Wang, Adsorption mechanism and improvements of the adsorption equation for adsorption refrigeration pairs, Int. J. Energy Res., 23 (1999) 887–898.
[29] S.Y. Wang, T. Vincent, C. Faur, E. Guibal, Alginate and algal-based beads for the sorption of metal cations: Cu(II) and Pb(II), Int. J. Mol. Sci., 17 (2016) 1453–1460.
[30] V.K. Gupta, R. Jain, M. Shrivastava, A. Nayak, Equilibrium and thermodynamic studies on the adsorption of the dye tartrazine onto waste "coconut husks" carbon and activated carbon, J. Chem. Eng., 55 (2010) 5083–5090.
[31] I.-G. Bacioiu, L. Stoica, C. Constantin, A.-M. Stanescu, Removal of tartrazine from aqueous solution by adsorption on activated red mud, Water Air Soil Pollut., 228 (2017) 298, https://doi.org/10.1007/s11270-017-3469-3.
[32] A. Murray, B. Örmeci, Competitive effects of humic acid and wastewater on adsorption of Methylene blue dye by activated carbon and non-imprinted polymers, J. Environ. Sci., 66 (2018) 310–317.
[33] B. Damiyine, B. Guenbour, R. Boussen, Adsorption of Rhodamine B dye onto expanded perlite from aqueous solution: kinetics, equilibrium and thermodynamics, J. Mater. Environ. Sci., 8 (2017) 345–355.
[34] C. Arora, S. Soni, S. Sahu, J. Mittal, P. Kumar, P.K. Bajpai, Iron based metal organic framework for efficient removal of Methylene blue dye from industrial waste, J. Mol. Liq., 284 (2019) 343–352.
[35] V.K. Gupta, S. Agarwal, R. Ahmad, A. Mirza, J. Mittal, Sequestration of toxic Congo Red dye from aqueous solution using ecofriendly guar gum/activated carbon nanocomposite, Int. J. Biol. Macromol., 158 (2020) 1310–1318.